hydrology

MDPI

Article

Monitoring Scour at Bridge Piers in Rivers with Supercritical Flows

Camilo San Martin [1], Cristian Rifo [1], Maricarmen Guerra [1], Bernd Ettmer [2] and Oscar Link [1,*]

[1] Civil Engineering Department, Faculty of Engineering, Universidad de Concepción, Concepción 4030000, Chile; casanmartin2017@udec.cl (C.S.M.); crisrifo@udec.cl (C.R.); marguerra@udec.cl (M.G.)
[2] Civil Engineering Department, Faculty of Engineering, Magdeburg-Stendal University of Applied Sciences, 39114 Magdeburg, Germany; bernd.ettmer@h2.de
* Correspondence: olink@udec.cl; Tel.: +56-41-2204447

Abstract: Bridges crossing rivers wider than 50 m are typically supported by piers. In a mobile riverbed, scour occurs around bridge piers, and it is the main cause of bridge collapses worldwide, especially during floods. While bridge pier scour has been extensively studied, there is still a lack of measuring systems for scour monitoring in the field. In this paper, we present existing devices for scour measurement and analyze their comparative advantages and disadvantages. A study case with a scoured bridge pier in supercritical flow is presented. Results show that supercritical flow patterns previously reported at the laboratory scale also occur in the field. The measured scour supports the hypothesis that supercritical flows, even when having high flow speeds, do not produce higher scour than subcritical flows. A possible explanation linked with the sediment sizes of rivers with supercritical flows is discussed. Further, field measurements of scour around bridge piers are needed to enhance our understanding of this complex and nearly unexplored situation.

Keywords: river engineering; floods hydrology; sediment transport

1. Introduction

Scour at bridge elements affects the load-carrying capacity of pier foundations (e.g., [1]). In extreme cases, i.e., when scour exceeds the design condition, the bridge pier can collapse, and with it, the superstructure. In fact, scour is one of the main causes of bridge collapse worldwide [2,3].

An important body of research has been conducted during recent decades to detect and understand the mechanisms of scour at bridge piers [4–7], to predict scour depth in different sediments [8–12], to perform the scour simulation numerically [13–20], to reproduce field scour in physical scale models [21–24], and to design countermeasures to prevent scour [25,26]. All of the aforementioned studies were conducted with piers exposed to subcritical flows. There has been little attention dedicated to understanding scour at piers in supercritical flows [27–29]. However, a number of bridge collapses occurring in the past have been described, e.g., [30,31].

Recognizing that scour is a stochastic process and the need for a different design approach, Rifo et al. [32] proposed a new design methodology based on the exceedance probability of maximum scour depth. Interestingly, Rifo et al. [32] showed that current design practices are not consistent in their bridge failure probability.

A possible way forward to enhance the current understanding of scour during floods is through appropriate field scour monitoring that provides information on the scouring process under field conditions. A number of scour monitoring devices and methods are available, and have been reviewed by Deng and Cai [33], including radar, sonar, time-domain reflectometry with fiber Bragg grating sensors, and sliding magnetic collars, and by Pendergast and Gavin [34], including so-called single-use devices such as float-out devices and tethered buried switches, pulse or radar devices, fiber Bragg grating, driven or buried

Citation: San Martin, C.; Rifo, C.; Guerra, M.; Ettmer, B.; Link, O. Monitoring Scour at Bridge Piers in Rivers with Supercritical Flows. *Hydrology* **2023**, *10*, 147. https://doi.org/10.3390/hydrology10070147

Academic Editor: Ezio Todini

Received: 14 June 2023
Revised: 10 July 2023
Accepted: 11 July 2023
Published: 13 July 2023

rod devices, sound wave devices, and electrical conductivity devices. Kazemian et al. [35] distinguished between so-called traditional monitoring methods including fathometers, ground penetrating radars, tilt sensors, electrical conductivity probes, magnetic sliding collars, and float-out devices, from vibration-based methods, focusing on accelerometers installed at the bridge pier. Indirect measurements in the context of structural health monitoring have been developed in recent years. Such approaches rely on monitoring the natural frequency of a bridge to detect changes caused by scour [36]. Frequency-based scour detection has been a focus of recent investigations, e.g., [37–41]. Monitoring techniques and devices that have been successfully applied for the analysis of scour under extreme field conditions, i.e., floods, include those described in the following sections.

1.1. Numbered Bricks

This scour measurement technique consists in placing a column of numbered bricks underneath the riverbed using an excavator prior to flood events. The brick column is typically located away from structures, and its location is indicated by a visible marker (e.g., a stick). After a flood has receded, the brick column is inspected to determine the number of bricks mobilized by a flood. Following the inspection, the scour depth at the column location is obtained based on the remaining number of bricks. This technique has been successfully applied in the field to measure scour in the vicinity of bridge piers or other river structures [42].

Lu et al. [43] measured scour on the Si-Lo Bridge in the lower Cho-Shui River, Taiwan, to validate a time-varying scour model under unsteady flow. They propose a total-scour model that incorporates local, general, and contraction scour. The authors used three methods to measure scour in the field: a sliding magnetic collar and a steel rod were installed in bridge piers located mid-channel to measure the total scour, and a numbered brick column was installed upstream of the bridge to determine general scour. The results showed that all three methods were successful in measuring scour during two extreme flood events.

Su and Lu [44] successfully used a numbered brick column to measure short-term general scour during floods in two steep rivers located in Taiwan, namely the Cho-Shui River and the Dajia River. Up to 90 numbered bricks at a time were installed to record maximum scour depth, and scour was measured during four different floods, with maximum discharge above 2000 m^3/s. The authors reported that for a low-flow flood (700 m^3/s), only the top brick was moved, noting that the discharge was not enough to initiate scour at the site.

Yang and Su [45] used the numbered brick technique in tandem with a wireless tracer to monitor scour in real time. The measuring system consisted in installing round-shaped buoyant wireless tracers equipped with a radio signal transmitter at different depths within the brick column. This method was used in the same intermittent Cho-shui River in Taiwan, between the Mingchu Bridge and the Formosa Super Highway Bridge, during a flood. Authors were able to track the initiation of movement of only one of the wireless tracers during the flood, since the rest of the tracers were too deep within the brick column to be released.

Despite being widely used, the brick column method solely provides the maximum scour depth once the flood has ended and does not allow for an estimation of the scouring process over time. Note that all these applications occurred in intermittent rivers where it is relatively easy to excavate and to install the bricks prior to a flood.

1.2. Distance Sensors for Scour Measurement

Scour monitoring can also be carried out using sonars and radars that monitor the scour depth on time. However, these techniques are often limited to low flow velocities, low flow depths, and/or low suspended sediment matter (SSM) concentrations. Ultrasonic sensors use active acoustics to estimate the distance from the instrument to a solid boundary. The acoustic returns might be affected by the presence of bubbles and particles through the water column. Progress has been made to detect the fixed bottom using acoustic instruments under high SSM by separating the acoustic returns of moving particles from those of fixed particles (i.e., the bottom) [46,47].

Sturm et al. [48] used multiple fathometers (i.e., echo-sounders or sonars) for monitoring bridge pier scour at four different bridges in Georgia, the United States. The time evolution of bridge pier scour holes was successfully measured during small to moderate floods, i.e., with return periods of less than 2 years.

Yu et al. [49] introduced a comparative study of the Time Domain Reflectometry (TDR) method and the ultrasonic method for scour measurements. This study indicates that both the TDR and ultrasonic methods can provide accurate measurements of scour depth.

Wu et al. [50] showed that a monitoring system based on ultrasonic sensors can measure scour depths. Link et al. [51] used an ultrasonic distance sensor for monitoring maximum scour depth at a bridge pier in the Rapel River, in Chile, during a six-day period, while daily floods occurred due to hydropeaking produced by an existing Rapel hydropower dam located upstream of the bridge. The measurement results showed that the scour sensor can be applied to clear-water rivers.

Scour monitoring systems are expensive, and for that reason, methods are required to guide decision-makers to decide if the installation of a monitoring system is appropriate or not. In the following section, Materials and Methods, a challenging case involving a bridge located in a steep mountain river reach with a supercritical flow is presented, together with the measuring techniques that we applied. The obtained measured results are presented and discussed.

2. Materials and Methods

2.1. Study Site

The Rucúe Bridge is located in central Chile (71°79′72″ W y 37°34′32″ S) over the Rucúe River. The bridge was built in 1970 and has two concrete rectangular piers aligned with the flow and spaced 21 m apart. The study pier (Pier #1) is 2.9 m in width and 9 m in length. A 178.4 MW hydropower plant located 6.2 km downstream of the bridge started its construction and began operations in 1998. The hydropower plant water intake is located 7.2 km upstream of the Rucúe Bridge, diverting part of the river discharge after 1998. Figure 1a,b show the location of the river watershed in Chile, the hydropower plant intake, and the Rucúe Bridge. Figure 1c shows a schematic view of the river cross section with the bridge, including a river bathymetry from April 2022 (note the scour at study Pier #1).

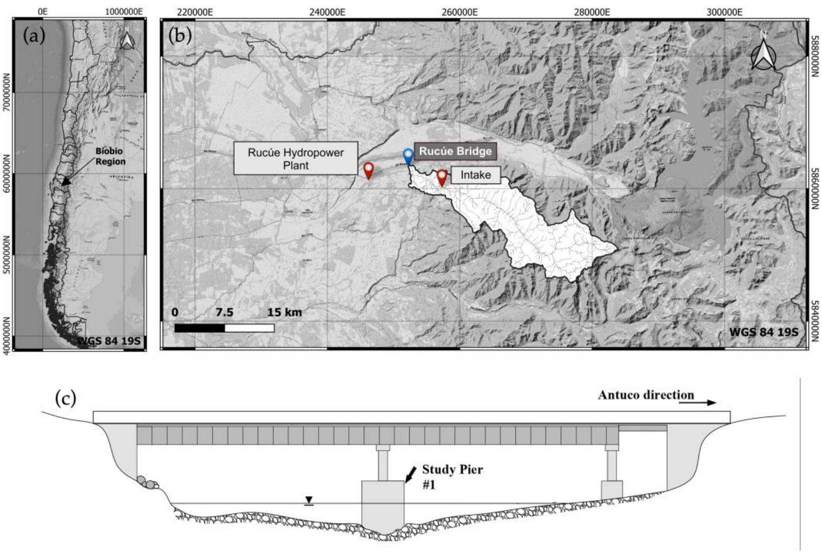

Figure 1. Location of the study site: (**a**) map of Chile and Biobío region. (**b**) Rucúe watershed and study bridge. (**c**) Schematic of Rucúe River cross section and bridge, the studied pier, and river bathymetry.

Bridge properties and Rucúe River information are presented in Table 1. Figure 2 shows the grain size distribution of the riverbed sediments at the Rucúe Bridge cross section obtained using the Wolman (1954) method for coarse granular soil. A sample of 100 pebbles was collected upstream and downstream of the bridge pier. The pebbles' axes were measured in the field and used to construct the sieve curve. The sediment size distribution is unimodal, and the riverbed is composed of pebbles with a d_{50} equal to 145 mm and a d_{90} equal 335 mm, and the geometric standard deviation of the sediment grain size is equal to 1.93 mm.

Table 1. Properties of the bridge and study site.

Property	Value
Bridge geometry	Rectangular
Bridge length (m)	51
Number of piers	2
Bridge span (m)	21
Pier #1 width (m)	2.9
Drainage area (km^2)	211.73
Channel slope	~1.2%
Bed material	pebbles

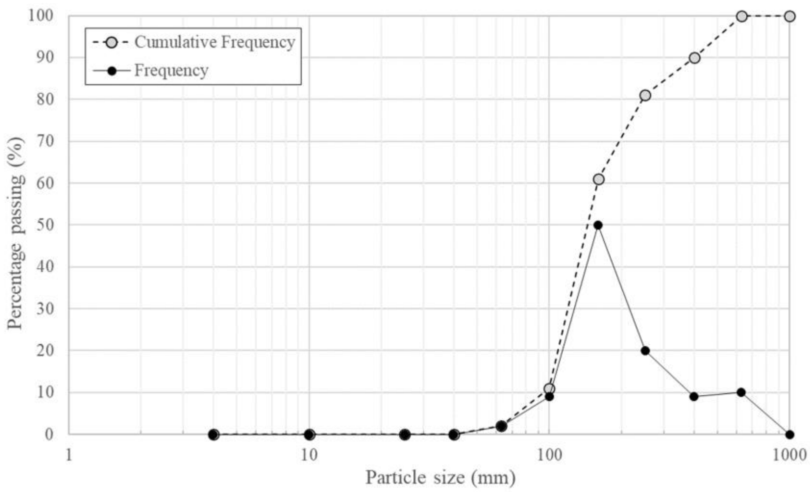

Figure 2. Grain size distribution of the riverbed sediments at Rucúe Bridge cross section.

Streamflow data are available from the gauge station Río Rucúe at Camino a Antuco (administered by Chile's Dirección General de Aguas (DGA)) between 1985 and 2020, with a data gap between 2010 and 2012. This gauge is located at the Rucúe Bridge. Figure 3 shows the hydrograph at Rucúe Bridge from 1985 to 2020.

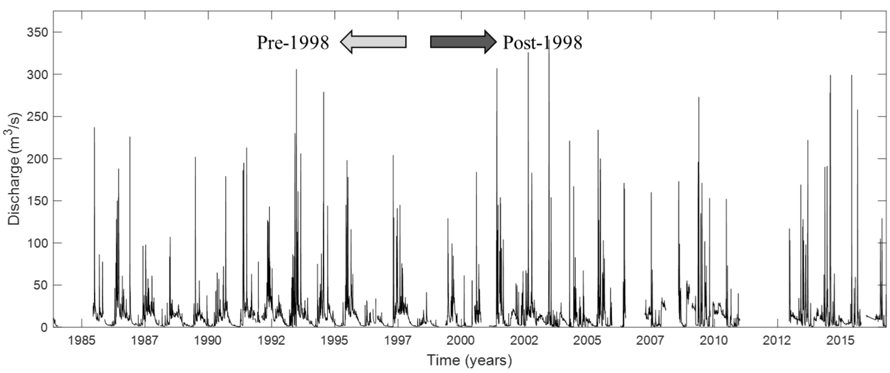

Figure 3. Hydrograph at Rucúe Bridge from 1985 to 2020 from DGA *Rucúe en Puente Camino a Antuco* gauge station.

Even when the Rucúe River drains a mountain area of the Andes, the hydrograph reveals that the hydrologic regime is pluvial, with the highest discharges caused by rainfalls during the rainy season in the wintertime, from June to September. Snowfall contribution to river discharge is small and occurs mainly in the form of baseflow.

2.2. Data Collection

2.2.1. Streamflow

Discharge measurements were conducted using an RDI StreamPro 2 MHz acoustic Doppler current profiler (ADCP) in a cross section immediately upstream of the study bridge. The ADCP was mounted down-looking on board a small boat (Figure 5c) and moved across the river while measuring bottom-track velocities and water velocity through the water column at 1 Hz using 7 cm depth cells. Simultaneously, flow depth was measured using a pressure sensor (HOBO, U20-001-01) with a sampling frequency of 15 min and a precision of ± 0.5 cm.

These data were used to construct a rating curve to estimate streamflow data from 2022 onwards, and to be used in future riverbed analysis. The rating curve was determined from the flow depth and discharge measured for the present study. A one-dimensional Rucúe River reach model was constructed in Hec-Ras to further populate and extrapolate the rating curve at the bridge location. The model considered an up-to-date topo-bathymetry obtained for this study.

To determine the flow regime, a local Froude number, Fr, was estimated as:

$$Fr = \frac{U}{\sqrt{g\,h}}, \tag{1}$$

where U is the depth-averaged horizontal flow speed, h is the local water depth, and g is the gravity acceleration, equal to 9.81 $\mathrm{m/s^2}$. In addition, a maximum Froude number was estimated using the maximum horizontal flow speed at each measurement point.

2.2.2. Scour Measurements

Existing scour was measured in April 2022. The scour hole around bridge Pier #1 was measured using a 5 m long limnimeter with an approximate precision of ± 1 cm (due to the oscillating water column and the ruler's round edges). The measurement technique consisted of vertically submerging the limnimeter into the flow and recording the water depth once the limnimeter reached the bottom of the bed. Figure 4a shows a photograph taken during the measurement procedure.

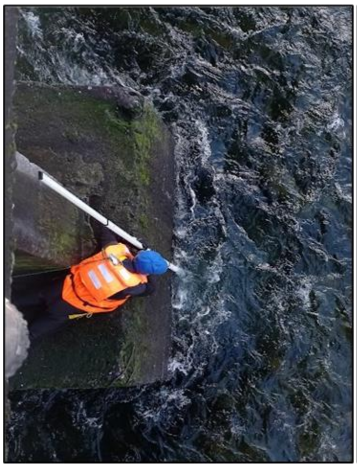

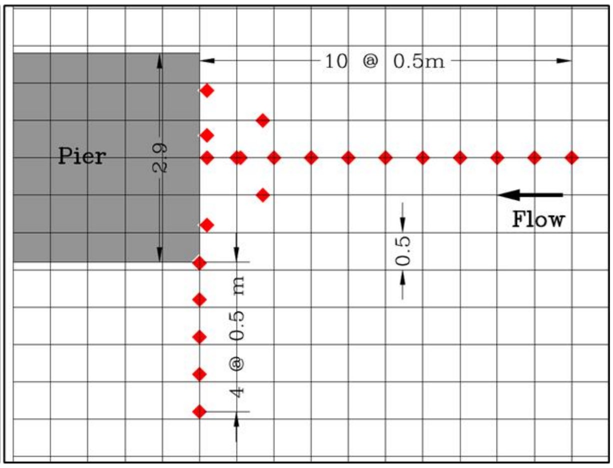

Figure 4. Scour measurement using a limnimeter: photograph of performing the measurement (**left**). Scheme of measuring points (**right**).

Scour depth measurements were taken at several points around the scour hole upstream of Pier #1. Measurement points were located along two main axes: one parallel to the flow direction beginning at the center of the study pier, and one axis in the cross-river direction located immediately upstream of the bridge pier. Additional measurements were taken within the scour hole to capture its shape. Most records were taken every 0.5 m, and the distribution of measurement points is shown in Figure 4.

The time evolution of scour upstream of Pier #1 of the Rucúe Bridge is currently being monitored with an Airmar Echorange SS510 ultrasonic scour sensor. The scour sensor is located at the center of Pier #1 at a distance of 25 cm from the pier wall and 20 cm from the bottom. The scour depth corresponds to the average depth of an area equal the sensor area (a circle 70 mm in diameter) that increases with depth, as the ultrasound signal widens along the traveling distance to the bottom with an angle of 9°. The sensor is set to measure the distance to the bottom every 10 min with a 1 cm precision, equivalent to 0.07 times the riverbed d50. The aim is to obtain scour variation during the 2023 winter floods. A pressure sensor (HOBO, U20-001-01) is also installed well outside the scour hole to measure the flow depth every 10 min in order to estimate discharge using the previously obtained rating curve.

Figure 5 shows the Rucúe Bridge during low (a) and high (b) flows, the ADCP and small vessel used for the velocity and discharge measurements (c), the pressure sensor used to measure water depth installed during low streamflow (d), and the installed scour sensor (e).

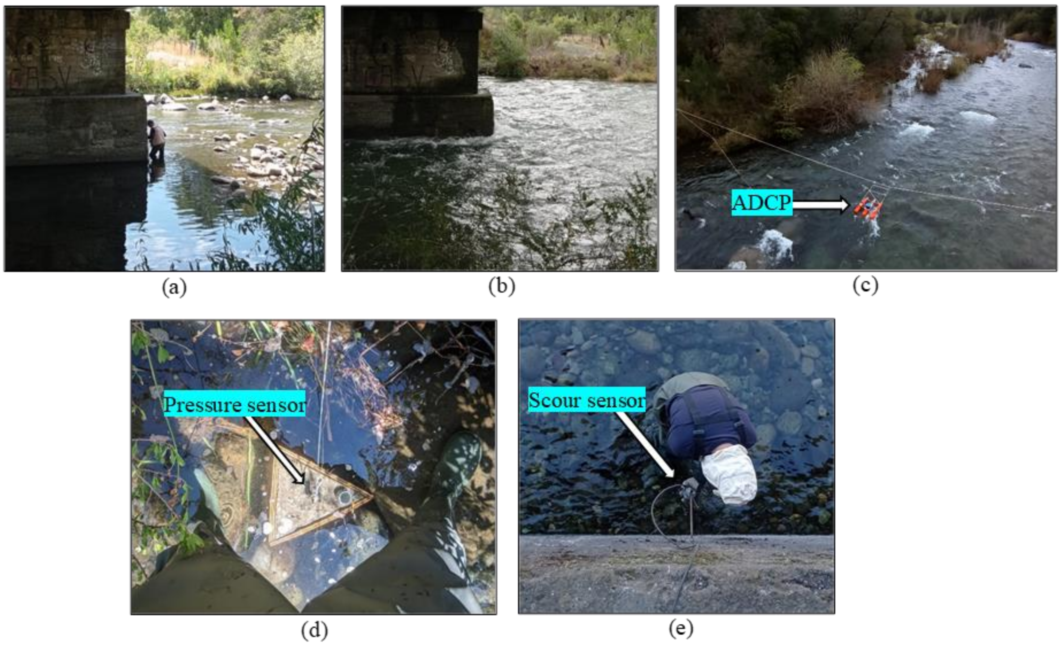

Figure 5. Rucúe Bridge Pier #1 during low (**a**) and high (**b**) flows, the ADCP for velocity flow field and discharge measurements (**c**), the water pressure sensor for flow depth measurement (**d**), and the installed scour sensor (**e**).

3. Results

3.1. Flow Regime

Figure 6a shows the velocity distribution obtained with the vessel-mounted ADCP just upstream of the Rucúe Bridge for a 15 m^3/s discharge measured on 9 September 2022. As expected, the flow speed and water depth varied across the river section. The maximum speed was about 1.7 m/s 12 m from the right river shore (study Pier #1 is located 11 m from the right river shore).

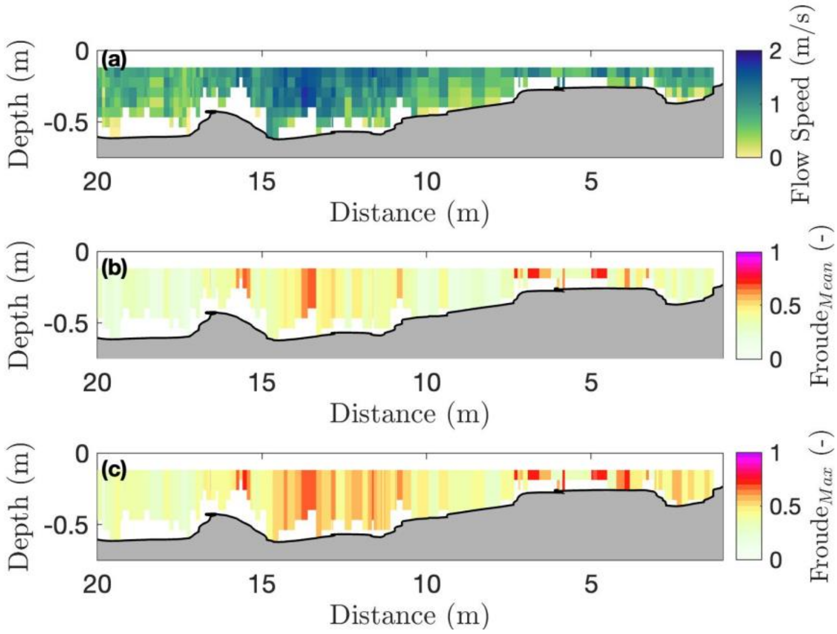

Figure 6. Velocity measurements and Froude number in a cross section when discharge was 15 m^3s^{-1}. (**a**) Flow speed, (**b**) Mean Froude number for each water column, and (**c**) maximum Froude number for each water column.

The computed Froude number is shown in Figure 6b, and the maximum Froude number is shown in Figure 6c. It is observed that the local Froude number varies across the river section, and it is greater than 0.7 in the pier vicinity (11 m from the right river shore); thus, it is expected that supercritical flow will occur during floods with discharges higher than 15 m^3/s.

3.2. Supercritical Flow Patterns

Evidence of supercritical flow patterns around the study pier was observed at the Rucúe Bridge during a 64 m^3/s winter flood that occurred on 1 July 2022. Unfortunately, velocity measurements were not obtained on this day due to safety issues that arose when installing the ADCP tag lines. As shown in Figure 7, a detached hydraulic jump formed immediately upstream of the bridge pier, and a small bow wave is observable on top of the jump. From laboratory experiments, Riviere et al. [52] described two different free-surface patterns that form in front of a rectangular pier during supercritical flow: the wall-jet-like bow wave and the detached hydraulic jump. The formation of each pattern depends on the ratio of water depth and pier width, and on the Froude number. According to Riviere et al. [52], considering an approximate 0.8 m water depth and a 2.9 m pier width, together with the observed hydraulic jump, the corresponding Froude number should be between 1 and 1.6 for this flood.

3.3. Existing Scour

Figure 8 shows the scour hole measured during April 2022 using a limnimeter. The scour shape in the Rucúe riverbed, which is composed of pebbles, is similar to the typical scour hole shape, forming a circular hole around the obstacle. The measured scour slope exhibits a knick point at 3 m upstream of the pier wall, and three regions with different slopes are identifiable, resembling the horseshoe vortex structure, with a corner vortex close to the pier wall, an active region in the middle of the scour hole with a high slope angle, and a third, less active region with a slope angle close to the repose angle of the sediment particles. The study pier presents a maximum scour depth of 2.05 m, which is 0.71 times the pier width.

Figure 7. Supercritical flow pattern observed around bridge Pier #1 for a 64 m^3/s discharge. (**a**) shows a view of Pier#1 from the right bank. (**b**) shows a view of Pier#1 from the left bank.

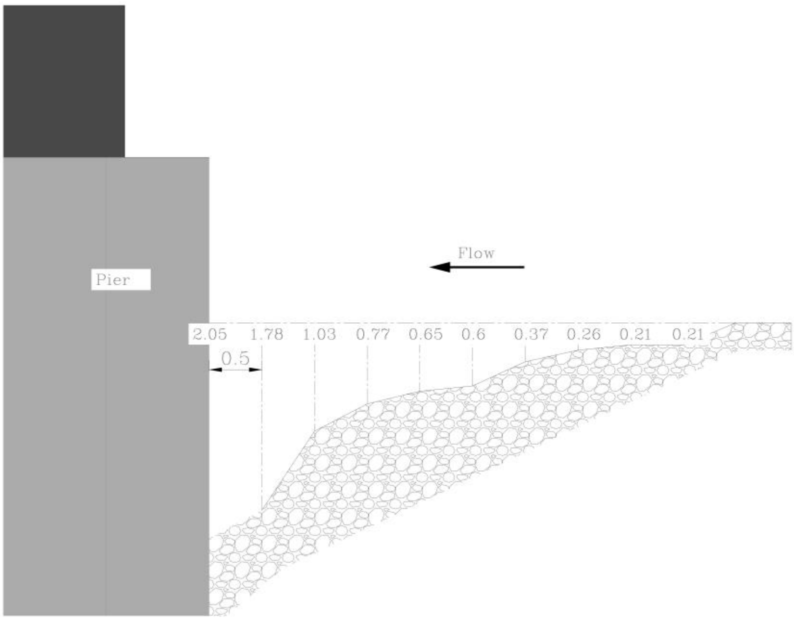

Figure 8. Scour hole as of April 2022 measured using a 5 m limnimeter. Numbers indicate the scour depth upstream of the pier in m. Depths are reported every 50 cm along a mid-pier axis perpendicular to the pier in the flow direction.

4. Discussion

Measuring devices and techniques for the characterization of pier scour in the field were revised, and a field measurement of scour at a pier in a supercritical flow was analyzed. In the following, presented results are discussed regarding flow patterns causing scour in supercritical flows, scour hole shape, and maximum scour depth. As the literature on scour at piers in supercritical flows is scarce, the following discussions also present some comparisons with the better-known cases of scour at piers in subcritical flows.

Mignot et al. [52] and Riviere et al. [53] described the flow patterns at piers in a fixed bed with supercritical flows, distinguishing two flow patterns, namely the detached hydraulic jump pattern and the wall-jet-like bow wave pattern. The observed flow pattern in supercritical flows at Pier #1 of the Rucúe Bridge, shown in Figure 7, coincided well with the patterns reported for laboratory [53] and field [28] situations, confirming the occurrence of a detached hydraulic jump following the threshold criteria reported by [52].

The measured shape of the scour hole at Pier #1 of the Rucúe Bridge was formed in a riverbed composed of pebbles and exhibited a similar shape to scour holes in sand [54] and gravel [55]. Moreover, the measured scour slope also exhibited a knick point, as was reported for sediments finer than pebbles [5,56].

Since its construction in 1970, i.e., after 53 years in service, the study pier, Pier #1, presents a maximum scour depth of 2.05 m, which is 0.71 times the pier width, and much smaller than the equilibrium scour depth that one would expect around a pier in a subcritical flow when applying scour formulas. Unfortunately, there is no available information on maintenance performed on and eventual re-filling of the scour hole around the study pier during its service life, to certainly determine if the measured maximum scour was caused by the 53-year-long hydrograph during the service life of the bridge or if it formed after some maintenance work. However, the measured scour depth is consistent with those measured by Mignot et al. [27] and Roux et al. [29], supporting the hypothesis that the observed scour was formed during several high-water events that have occurred since the bridge construction.

An important open question that has already been stated by [27–29] is the possibility that scour in supercritical flows achieves magnitudes comparable to those of scour in subcritical flows, which the obtained results support. A possible explanation is that supercritical flows occur in steep rivers, where, at the same time, bed shear stress is, in general, higher than in mild-slope river reaches with subcritical flows, as bed shear stress increases with bed slope. Consequently, the sediment transport capacity and stream power is expected to be much higher in rivers with supercritical flows than in river reaches with subcritical flows. Nevertheless, steep river reaches exhibit, naturally, much coarser sediment beds than mild-slope reaches, as natural sediment size sorting occurs. It appears then evident that their higher transport capacity does not produce a higher scour in the coarser riverbeds observed in steep river reaches. In fact, the scour controlling parameter called flow intensity, which is defined as the average flow velocity divided by the critical velocity for initiation of sediment transport [57], remains similar in both flow regimes, and thus, scour depth is also similar in both regimes. The existence of internal flow mechanisms that reduce the erosive power of the flow around obstacles in supercritical flows by damping the horseshoe vortex appears plausible in the wall-jet-like bow wave flow pattern, but further research is needed to verify this idea.

5. Conclusions

Existing devices for scour measurement were revised and their comparative advantages and disadvantages were analyzed. The ultrasonic distance sensor appeared to be a better alternative than other simple techniques such as numbered bricks or limnimeters, as it allows a continuous measurement in time. Further, results on the scour observed at a bridge pier in a steep river reach, i.e., with supercritical flows, was presented.

Supercritical flow patterns previously reported at the laboratory scale also occurred in the field. In particular, the detached hydraulic jump was observed at Pier #1 of the Rucúe Bridge.

The measured scour hole geometry supports the hypothesis that supercritical flows, even when having high flow speeds, do not produce higher scour than subcritical flows. A possible explanation linked with the sediment sizes of rivers with supercritical flows was discussed.

Further, field measurements of scour around bridge piers are needed to enhance our understanding of this complex and nearly unexplored situation.

Author Contributions: The contributions of each author to the research are as follows: conceptualization, M.G., O.L. and B.E.; methodology, C.S.M., M.G. and O.L.; field data acquisition, C.S.M., M.G., O.L. and C.R.; writing—original draft preparation, C.S.M., M.G. and O.L.; writing—revision and editing, B.E. and C.R.; supervision, O.L.; project administration, O.L. All authors have read and agreed to the published version of the manuscript.

Funding: This research was funded by Agencia Nacional de Investigación y Desarrollo ANID, grant Fondecyt Nr. 1221341: "Scour at Bridge Piers in Supercritical Flows".

Data Availability Statement: All data generated and used during the study appear in the published article. Related information is available from the corresponding author by request.

Acknowledgments: The valuable support and help of our technician René Iribarren and MSc students Benjamín Durán and Bastián Martínez during the field campaigns is especially acknowledged.

Conflicts of Interest: The authors declare no conflict of interest.

References

1. Fitzgerald, P.C.; Malekjafarian, A.; Cantero, D.; OBrien, E.J.; Prendergast, L.J. Drive-by Scour Monitoring of Railway Bridges Using a Wavelet-Based Approach. *Eng. Struct.* **2019**, *191*, 1–11. [CrossRef]
2. Melville, B.W.; Coleman, S.E. *Bridge Scour*; Water Resources Publications: Littleton, CO, USA, 2000; ISBN 9781887201186.
3. Pizarro, A.; Manfreda, S.; Tubaldi, E. The Science behind Scour at Bridge Foundations: A Review. *Water* **2020**, *12*, 374. [CrossRef]
4. Apsilidis, N.; Diplas, P.; Dancey, C.L.; Bouratsis, P. Time-Resolved Flow Dynamics and Reynolds Number Effects at a Wall-Cylinder Junction. *J. Fluid Mech.* **2015**, *776*, 475–511. [CrossRef]
5. Dargahi, B. Controlling Mechanism of Local Scouring. *J. Hydraul. Eng.* **1990**, *116*, 1197–1214. [CrossRef]
6. Chen, Q.; Qi, M.; Zhong, Q.; Li, D. Experimental Study on the Multimodal Dynamics of the Turbulent Horseshoe Vortex System around a Circular Cylinder. *Phys. Fluids* **2017**, *29*, 15106. [CrossRef]
7. Soto, J.; Link, O.; Brevis, W. Elucidating the Importance of Sediment Avalanches in Scour at Obstacles. *J. Hydraul. Res.* **2022**, *60*, 62–73. [CrossRef]
8. Arneson, L.A.; Zevenbergen, L.W.; Lagasse, P.F.; Clopper, P.E. *Evaluating Scour at Bridges*, 5th ed.; Associates, A., Ed.; U.S. Department of Transportation: Washington, DC, USA, 2012. Available online: https://rosap.ntl.bts.gov/view/dot/42053 (accessed on 10 June 2023).
9. Sheppard, D.M.; Melville, B.; Demir, H. Evaluation of Existing Equations for Local Scour at Bridge Piers. *J. Hydraul. Eng.* **2014**, *140*, 14–23. [CrossRef]
10. Qi, W.G.; Gao, F.P.; Randolph, M.F.; Lehane, B.M. Scour Effects on p–y Curves for Shallowly Embedded Piles in Sand. *Géotecnique* **2016**, *66*, 648–660. [CrossRef]
11. Link, O.; Castillo, C.; Pizarro, A.; Rojas, A.; Ettmer, B.; Escauriaza, C.; Manfreda, S. A Model of Bridge Pier Scour during Flood Waves. *J. Hydraul. Res.* **2017**, *55*, 310–323. [CrossRef]
12. Pizarro, A.; Ettmer, B.; Link, O. Relative Importance of Parameters Controlling Scour at Bridge Piers Using the New Toolbox ScourAPP. *Comput. Geosci.* **2022**, *163*, 105117. [CrossRef]
13. Paik, J.; Escauriaza, C.; Sotiropoulos, F. On the Bimodal Dynamics of the Turbulent Horseshoe Vortex System in a Wing-Body Junction. *Phys. Fluids* **2007**, *19*, 45107. [CrossRef]
14. Paik, J.; Escauriaza, C.; Sotiropoulos, F. Coherent Structure Dynamics in Turbulent Flows Past In-Stream Structures: Some Insights Gained via Numerical Simulation. *J. Hydraul. Eng.* **2010**, *136*, 981–993. [CrossRef]
15. Escauriaza, C.; Sotiropoulos, F. Initial Stages of Erosion and Bed Form Development in a Turbulent Flow around a Cylindrical Pier. *J. Geophys. Res. Earth Surf.* **2011**, 116. [CrossRef]
16. Link, O.; González, C.; Maldonado, M.; Escauriaza, C. Coherent Structure Dynamics and Sediment Particle Motion around a Cylindrical Pier in Developing Scour Holes. *Acta Geophys.* **2012**, *60*, 1689–1719. [CrossRef]
17. Schanderl, W.; Manhart, M. Reliability of Wall Shear Stress Estimations of the Flow around a Wall-Mounted Cylinder. *Comput. Fluids* **2016**, *128*, 16–29. [CrossRef]
18. Schanderl, W.; Jenssen, U.; Manhart, M. Near-Wall Stress Balance in Front of a Wall-Mounted Cylinder. *Flow Turbul. Combust.* **2017**, *99*, 665–684. [CrossRef]
19. Quezada, M.; Tamburrino, A.; Niño, Y. Numerical Simulation of Scour around Circular Piles Due to Unsteady Currents and Oscillatory Flows. *Eng. Appl. Comput. Fluid Mech.* **2018**, *12*, 354–374. [CrossRef]
20. Quezada, M.; Tamburrino, A.; Niño, Y. Numerical Study of the Hydrodynamics of Waves and Currents and Their Effects in Pier Scouring. *Water* **2019**, *11*, 2256. [CrossRef]
21. Ettema, R.; Melville, B.W.; Barkdoll, B. Scale Effect in Pier-Scour Experiments. *J. Hydraul. Eng.* **1998**, *124*, 639–642. [CrossRef]
22. Ettema, R.; Kirkil, G.; Muste, M. Similitude of Large-Scale Turbulence in Experiments on Local Scour at Cylinders. *J. Hydraul. Eng.* **2006**, *132*, 33–40. [CrossRef]
23. Lee, S.O.; Sturm, T.W. Effect of Sediment Size Scaling on Physical Modeling of Bridge Pier Scour. *J. Hydraul. Eng.* **2009**, *135*, 793–802. [CrossRef]
24. Link, O.; Henríquez, S.; Ettmer, B. Physical Scale Modelling of Scour around Bridge Piers. *J. Hydraul. Res.* **2019**, *57*, 227–237. [CrossRef]
25. Tao, J.; Li, J.; Wang, X.; Bao, R. Nature-Inspired Bridge Scour Countermeasures: Streamlining and Biocementation. *J. Test. Eval.* **2018**, *46*, 1376–1390. [CrossRef]

26. Singh, R.K.; Pandey, M.; Pu, J.H.; Pasupuleti, S.; Villuri, V.G.K. Experimental Study of Clear-Water Contraction Scour. *Water Supply* **2020**, *20*, 943–952. [CrossRef]
27. Mignot, E.; Moyne, T.; Doppler, D.; Rivière, N. Clear-Water Scouring Process in a Flow in Supercritical Regime. *J. Hydraul. Eng.* **2016**, *142*, 4015063. [CrossRef]
28. Link, O.; Mignot, E.; Roux, S.; Camenen, B.; Escauriaza, C.; Chauchat, J.; Brevis, W.; Manfreda, S. Scour at Bridge Foundations in Supercritical Flows: An Analysis of Knowledge Gaps. *Water* **2019**, *11*, 1656. [CrossRef]
29. Roux, S.; Link, O.; Riviere, N.; Mignot, E. Live-Bed Pier Scour in Supercritical Open-Channel Flows. *J. Hydraul. Res.* **2022**, *60*, 675–685. [CrossRef]
30. Quetelard, H.; Bessemoulin, P.; Cerveny, R.S.; Peterson, T.C.; Burton, A.; Boodhoo, Y. Extreme Weather: World-Record Rainfalls during Tropical Cyclone Gamede. *Bull. Am. Meteorol. Soc.* **2009**, *90*, 603–608. [CrossRef]
31. Roux, S.; Misset, C.; Romieu, P. *Construction of a New Bridge over the Rivière des Galets; Study on Physical Model; Phase 1—Tests on Abutment Scour*; CNR: Lyon, France, 2015.
32. Rifo, C.; Arriagada, P.; Ettmer, B.; Link, O. Frequency Analysis of Extreme Scour Depths at Bridge Piers and Their Contribution to Bridge Collapse Risk. *Hydrol. Sci. J.* **2022**, *67*, 2029–2041. [CrossRef]
33. Deng, L.; Cai, C.S. Bridge Scour: Prediction, Modeling, Monitoring, and Countermeasures—Review. *Pract. Period. Struct. Des. Constr.* **2010**, *15*, 125–134. [CrossRef]
34. Prendergast, L.J.; Gavin, K. A Review of Bridge Scour Monitoring Techniques. *J. Rock Mech. Geotech. Eng.* **2014**, *6*, 138–149. [CrossRef]
35. Kazemian, A.; Yee, T.; Oguzmert, M.; Amirgholy, M.; Yang, J.; Goff, D. A Review of Bridge Scour Monitoring Techniques and Developments in Vibration Based Scour Monitoring for Bridge Foundations. *Adv. Bridge Eng.* **2023**, *4*, 2. [CrossRef]
36. Sohn, H.; Farrar, C.R.; Hemez, F.M.; Shunk, D.D.; Stinemates, D.W.; Nadler, B.R.; Czarnecki, J.J. *A Review of Structural Health Monitoring Literature: 1996–2001*; Los Alamos National Laboratory: Los Alamos, NM, USA, 2003; Volume 1, p. 16.
37. Malekjafarian, A.; Kim, C.-W.; OBrien, E.J.; Prendergast, L.J.; Fitzgerald, P.C.; Nakajima, S. Experimental Demonstration of a Mode Shape-Based Scour-Monitoring Method for Multispan Bridges with Shallow Foundations. *J. Bridge Eng.* **2020**, *25*, 4020050. [CrossRef]
38. Prendergast, L.J.; Hester, D.; Gavin, K. Determining the Presence of Scour around Bridge Foundations Using Vehicle-Induced Vibrations. *J. Bridge Eng.* **2016**, *21*, 4016065. [CrossRef]
39. Xiong, W.; Cai, C.S.; Kong, B.; Zhang, X.; Tang, P. Bridge Scour Identification and Field Application Based on Ambient Vibration Measurements of Superstructures. *J. Mar. Sci. Eng.* **2019**, *7*, 121. [CrossRef]
40. Zhang, F.; Zang, Z.; Zhao, M.; Zhang, J.; Xie, B.; Zou, X. Numerical Investigations on Scour and Flow around Two Crossing Pipelines on a Sandy Seabed. *J. Mar. Sci. Eng.* **2022**, *10*, 2019. [CrossRef]
41. Tubaldi, E.; Antonopoulos, C.; Mitoulis, S.A.; Argyroudis, S.; Gara, F.; Ragni, L.; Carbonari, S.; Dezi, F.; Vratsikidis, A.; Pitilakis, D.; et al. Field Tests and Numerical Analysis of the Effects of Scour on a Full-Scale Soil–Foundation–Structural System. *J. Civ. Struct. Health Monit.* **2022**. [CrossRef]
42. Hong, J.H.; Guo, W.D.; Chiew, Y.M.; Chen, C.H. A New Practical Method to Simulate Flood-Induced Bridge Pier Scour-A Case Study of Mingchu Bridge Piers on the Cho-Shui River. *Water* **2016**, *8*, 238. [CrossRef]
43. Lu, J.-Y.; Hong, J.-H.; Su, C.-C.; Wang, C.-Y.; Lai, J.-S. Field Measurements and Simulation of Bridge Scour Depth Variations during Floods. *J. Hydraul. Eng.* **2008**, *134*, 810–821. [CrossRef]
44. Su, C.C.; Lu, J.Y. Measurements and Prediction of Typhoon-Induced Short-Term General Scours in Intermittent Rivers. *Nat. Hazards* **2013**, *66*, 671–687. [CrossRef]
45. Yang, H.C.; Su, C.C. Real-Time River Bed Scour Monitoring and Synchronous Maximum Depth Data Collected during Typhoon Soulik in 2013. *Hydrol. Process.* **2015**, *29*, 1056–1068. [CrossRef]
46. Hurther, D.; Thorne, P.D. Suspension and Near-bed Load Sediment Transport Processes above a Migrating, Sand-rippled Bed under Shoaling Waves. *J. Geophys. Res. Oceans* **2011**, *116*. [CrossRef]
47. Fromant, G.; Mieras, R.S.; Revil-Baudard, T.; Puleo, J.A.; Hurther, D.; Chauchat, J. On Bedload and Suspended Load Measurement Performances in Sheet Flows Using Acoustic and Conductivity Profilers. *J. Geophys. Res. Earth Surf.* **2018**, *123*, 2546–2562. [CrossRef]
48. Sturm, T.; Sotiropoulos, F.; Landers, M.; Gotvald, T.; Lee, S.; Ge, L.; Navarro, R.; Escauriaza, C. *Laboratory and 3D Numerical Modeling with Field Monitoring of Regional Bridge Scour in Georgia*; Georgia Department of Transportation Final Project; Georgia Department of Transportation: Atlanta, GA, USA, 2004.
49. Yu, X.; Yu, X. Laboratory Evaluation of Time-Domain Reflectometry for Bridge Scour Measurement: Comparison with the Ultrasonic Method. *Adv. Civ. Eng.* **2010**, *2010*, 508172. [CrossRef]
50. Wu, B.; Chen, W.; Li, H. Real-Time Monitoring of Bridge Scouring Using Ultrasonic Sensing Technology. In *Sensors and Smart Structures Technologies for Civil, Mechanical, and Aerospace Systems*; SPIE: Bellingham, WA, USA, 2012; Volume 8345, pp. 891–899. [CrossRef]
51. Link, O.; García, M.; Pizarro, A.; Alcayaga, H.; Palma, S. Local Scour and Sediment Deposition at Bridge Piers during Floods. *J. Hydraul. Eng.* **2020**, *146*, 4020003. [CrossRef]
52. Rivière, N.; Vouaillat, G.; Launay, G.; Mignot, E. Emerging Obstacles in Supercritical Open-Channel Flows: Detached Hydraulic Jump versus Wall-Jet-like Bow Wave. *J. Hydraul. Eng.* **2017**, *143*, 4017011. [CrossRef]

53. Mignot, E.; Riviere, N. Bow-Wave-like Hydraulic Jump and Horseshoe Vortex around an Obstacle in a Supercritical Open Channel Flow. *Phys. Fluids* **2010**, *22*, 117105. [CrossRef]
54. Link, O.; Pfleger, F.; Zanke, U. Characteristics of Developing Scour-Holes at a Sand-Embedded Cylinder. *Int. J. Sediment Res.* **2008**, *23*, 258–266. [CrossRef]
55. Diab, R.; Link, O.; Zanke, U. Geometry of Developing and Equilibrium Scour Holes at Bridge Piers in Gravel. *Can. J. Civ. Eng.* **2010**, *37*, 544–552. [CrossRef]
56. Hoffmans, G.; Verheij, H.J. *Scour Manual*; Routledge Balkema: London, UK, 1997.
57. Ettmer, B.; Orth, F.; Link, O. Live-Bed Scour at Bridge Piers in a Lightweight Polystyrene Bed. *J. Hydraul. Eng.* **2015**, *141*, 4015017. [CrossRef]